Development of PolyUAV: Polytechnic University's Unmanned Aerial Vehicle

Journal Paper

AUVSI Undergrad Competition

Presented By

David Jensen
Michael Roberts
Joseph Alifano
Thomas Szumczyk
William Cheung

May, 2004

Polytechnic University
Brooklyn, NY 11201

Abstract: *At Polytechnic University, an Autonomous Aerial Vehicle (UAV) Club is formed in September, 2003 and in less than one year, a fully functioning UAV system is developed and successfully tested to participate in the Association for Unmanned Vehicle Systems International (AUVSI) 2004 Student UAV Competition. The mechanical platform is a modified conventional radio controlled fixed wing airplane, ¼ scale J3 Piper cub. It is instrumented with autopilot system, MicroPilot 2028g, and additional mission specific sensors, such as sonar sensors for autonomous landing and cameras for reconnaissance, and communication equipments that are integrated into the MicroPilot. Various measures are taken for improved safety and fuel efficiency, and for the isolation of mechanical noise and electro-magnetic filed. The MicroPilot's automatic flight system has a two- layer hierarchical architecture, mission planning layer and feedback control layer for the mission execution. The feedback control system is decoupled into a set of Single-Input-Single-Output (SISO) subsystems and each subsystem is controlled by a Proportional-Integral-Derivative (PID) controller. In order to gain more insight into the dynamics of the vehicle system, and to choose appropriate initial conditions and control gains for robust flight, a comprehensive nonlinear model is developed for simulation. Then, the nonlinear model is linearized about each operating condition which will be set by the mission planning layer and various transfer functions are obtained for the robust tuning of PID gains. The PID controllers are first tested by simulation using the nonlinear model and then implemented on the UAV.*

1. Introduction

Aircrafts have been around for more than a century and in the last 50 year great efforts have been made to aid pilots or to completely remove pilots from the cockpit. The introduction of fly-by-wire systems has created an avenue for the advancements in developing autopilot systems. With the advancement of computer technologies, development of modern sensors and actuators, and breakthroughs in navigation technologies, completely Unmanned Aerial Vehicles (UAVs) have come from a concept to a reality. An Autonomous Aerial Vehicle is one that flies without any user input, while a UAV is an aircraft that does not carry a human operator, and can fly autonomously or be piloted remotely.

The demand for UAVs is growing rapidly mostly due to the military's drive to minimize the chances that soldiers are exposed to risks. In addition to being used for reconnaissance missions and as weapon systems for military, UAVs are finding civilian applications as well. This paper presents the development of a fully functioning prototype of an Unmanned Aerial Vehicle for the 2004 Student UAV competition hosted by the Association for Unmanned Vehicle Systems International (AUVSI). The vehicle is capable of performing a pre-programmed mission: (1) navigating to waypoints via GPS coordinates; (2) taking photographic footage to provide location, size, and orientation of the targets within the specified area (by GPS coordinates); (3) and then flying back to its home base and landing autonomously. The aircraft and its navigation and mission systems have been designed specifically to complete the mission designed by the competition.

2. Conceptual Design

To develop any autonomous unmanned vehicle system for general purposes or for a specific mission, no matter it is to be operated in the air, on the ground or under the water, first of all,

three major components need to be decided upon before further detailed developments: a) mechanical platform; b) computer system and sensors; and c) intelligent system architecture. Of course, in addition to the technical expertise of each team members and total manpower of the team, the time to finish and additional available resources such as budget and technical support from faculty members have to be considered when making decisions.

For the mechanical platform, three options were considered: a) an off-the-shelf radio controlled fixed wing airplane; b) an off-the-shelf radio controlled helicopter; and c) designing and building from scratch a fixed-wing airplane. Though all the team members have the expertise and we could get technical advice from faculty members, option (c) was immediately discarded since we thought we don't have enough time and enough manpower. We debated for a while between choices (a) and (b). Automating a helicopter appealed more to us since it was more challenging due to its much more complicated dynamics and inherent instability. However, it is much more costly, and much harder to maintain and manually fly which is needed during testing and emergency situations. In addition, as will be explained next, in the case of a helicopter, the development and integration of the computer system and sensors would take much more time in addition to it not being our team's expertise. Through the elimination process, we decided to go for the option of modifying an off-the-shelf fixed wing airplane. Considering the mission duration, expected payload and possible weather conditions during the mission, we decided to go for the ¼ scale J3 Piper cub.

For the computer system and sensor suits, we mainly considered two options: a) already integrated MicroPilot; and (b) home integration of navigation sensors, aerodynamics sensors, mission specific sensors and servo actuators with PC104 computer system. MicroPilot was chosen due to the compact size and the ease of an fully compact integrated system.

3. Description of Final Design: PolyUAV

3.1 Mechanical platform

The mechanical platform that we chose to instrument as a UAV is an off-the-shelf hobbyists' ¼ scale model, Hanger 9 J-3 Piper Cub, due to its high payload and other desirable characteristics for long range operation and instrumentation. It is a high wing aircraft and therefore, it can safely fly at very low speeds. The amount of cargo areas of the Piper Cub is ideal for placing large pieces of equipments in various locations throughout the aircraft. It also gives option of fabric cover versus monokote cover; fabric cover gives greater durability in the event of harsh landings and heavy wing loading. The engine that we chose is a Zenoah G-26, a two stroke single cylinder gasoline engine, due to it fuel efficient which is ideal for long range flights. The servos for the control surfaces are JR 537 dual ball bearing servos. These servos provide 45 oz torque at 0.12 seconds. Each aileron is fitted with its own servo as opposed to conventional configuration of single servo controlling both ailerons. All control surface gaps are sealed with a monokote plastic film to provide more accurate results from the control surfaces.

Figure 1. PolyUAV: Instrumented ¼ scale J3 Piper cub

3.2 Computer system and sensor suits

MicroPilot's MP2028^g system: It is an autopilot system with integrated navigation sensors such as GPS/INS as well as other aerodynamic sensors. The system has the ability to hold an altitude and navigate to pre-programmed coordinates. It can also be interfaced with off-the-shelf hobbyists' R/C systems for emergency handling and ease of system testing. In addition, the support of extensive data logging enables extensive post flight analysis.

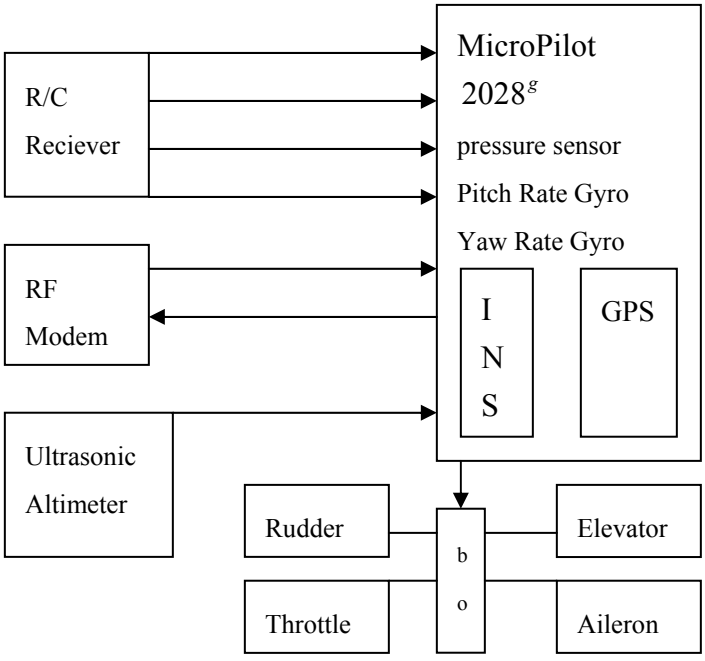

Figure 2: MicroPilot's MP2028^g

Sonar Senor: In order for the vehicle to land autonomously, it needs a low range altitude sensor; sonar was chosen for this task. Specifically an ultrasonic electrostatic sonar module and sensor were chosen. The principle by which it operates is that it will send a sound signal out and then listen for an echo. Utilizing the fact that a sound wave travels at .9 ft / millisecond the distance can be calculated and is done so by the MicroPilot.

Imaging System: A key element in reconnaissance is the ability to take clear and accurate pictures. Autonomous camera operation vs. video feed was taken into consideration. Of course an autonomous image acquisition system would be the most glamorous, but for the problem at hand it is overkill. All that must be done is to obtain images that will be clear enough to differentiate specific objects along with their orientation. For this reason we chose to use digital still cameras. The location of the cameras and the number of cameras on board to get accurate results also became an issue. It was decided that to maximum coverage two cameras will be used. The cameras are mounted in a gimbal housing that is located under the fuselage of the aircraft. The gimbal housing has the ability to keep the two cameras facing at the ground at all times. This will give us more accurate data and clearer pictures. The cameras will be controlled through an electronic switch via the MicroPilot board. The electronic switch has the ability to simultaneously activate the cameras. Another issue that became of importance that reflected on the camera system was the powering system that would be needed in order to power all of the equipment. Each subsystem received its own battery bank that consisted of a 5 cell 1500 MAH pack.

3.3 Communication system: The system of telemetry that we have chosen to outfit out UAV is a radio modem that is produced by MAX Stream. This is a 900Mhz radio modem with a range of up to 8 miles in clear sight. The Max Stream modem gives us the ability to have real time data on what the aircraft is doing during flight. It also gives us the communication link that allows us to change mission plans in flight.

4. Safety, Fuel Efficiency and Mechanical Vibration Isolation

With a prototype vehicle such as this, there are many concerns that arise throughout the design process. Since this vehicle houses sensitive electronic equipment considerations needed to be taken into account as far as the protection of this equipment. The main concern was to protect the MicroPilot Navigation System; not only from impact and vibration, but also from electromagnetic interference. The first challenge was to protect the MicroPilot from impact in the event that there is a catastrophic failure and the vehicle sustains a heavy impact. To deal with this problem a safe box was designed to house the equipment; a protective impact absorbing foam was chosen to shield the unit from any damage. In order for the safe box to be effective in protection from impact it would have to be fastened to the airframe so that it would not move in the event of an accident, as to prevent secondary impacts from taken place if say the MicroPilot was thrown from the aircraft.

Safety: Safety in dealing with any prototype is always a major concern, safety not only to the aircraft but also to the team on the ground. The bulk of the safety equipment is integrated into the ground station. The safety kit consists of the following components; first aid kit in the event of an accident to a team member, fire extinguisher abiding by guidelines posted by the AMA

National Model Aircraft Code regulations regarding running any gasoline style engine, and a preflight checklist. This Checklist involves all of the steps in sequential order to activate and expedite a UAV mission. Safety onboard the aircraft consists of a fault override in the event of a malfunction aboard the aircraft. There are two sequences of events that will take place. Scenario one; the aircraft looses radio reception from the transmitter. The aircraft will immediately switch over to computer in control mode and will start its last pre programmed mission and end with a circuit command. Second scenario is the aircraft sufferers from a fatal error. In the even that this happens the MicroPilot will activate right rudder, right roll, up elevation and close the throttle. This activation sequence will bring the aircraft to the ground in the quickest amount of time.

Protection from the electric waves: The next task was to protect the MicroPilot from electromagnetic waves that are emitted from the radio equipment on board. $1/8^{th}$ inch thick copper was chosen as the material for its ability to block electromagnetic waves, and its relatively low weight. Basically there are two parts to electromagnetic waves, that producing an electric field and that producing a magnetic field. Both must be dealt with because by Maxwell's equations if one exists, both exist and therefore stopping one will do nothing; both must be stopped. The electric field part is, in an ideal situation, fairly easy to deal with because an electric field (and therefore the electric part of an EM wave) cannot exist in a conducting shell with no openings. The problem however becomes more complicated when openings are introduced. An opening represents a break in shell and therefore something must be done. It actually turns out that the size of the opening allowed depends on the frequency with which one is trying to suppress. The higher the frequency the smaller the holes must be.

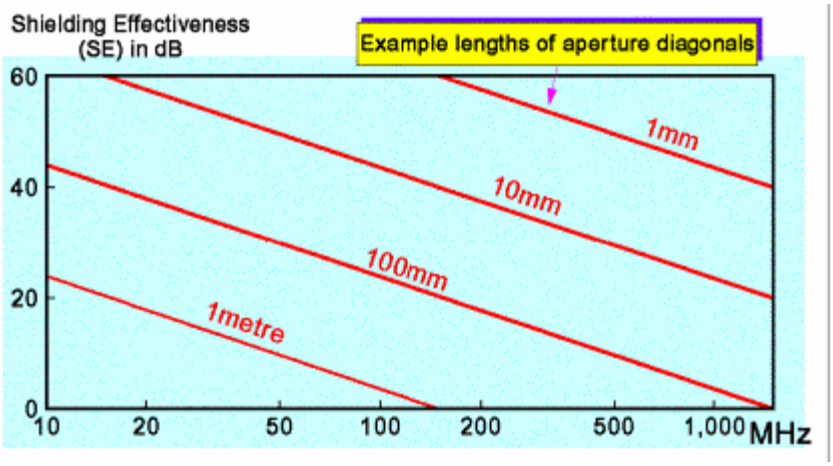

Figure: Rule of Thumb for the SE of Apertures

Also, sometimes it is necessary to have wires going into and out of the box. To deal with the interference that is admitted to the box by the skin of the wire (known as the skin affect), Ferrite Beads were used to shunt out the high frequency noise.

Protection from the magnetic waves: Now that the electric part of the interference has been dealt with it is now necessary to deal with the magnetic part of this interference. This turns out to be a little less trivial and unlike preventing an electric field where only the qualitative attribute of a material being a conductor is necessary, quantitative attributes such as thickness and magnetic permeability come into the picture. Essentially, if a shell is thicker and/or its permeability is

higher, it will more readily accept a magnetic field and therefore less of this field will be present inside. For the purposes in this project, copper was chosen; mainly for its low cost, however it does have a high magnetic permeability. The thickness was chosen mainly again for the weight issue and what is available, nevertheless it was necessary to make sure that the requirement for thickness depending on frequency was met, and it was.

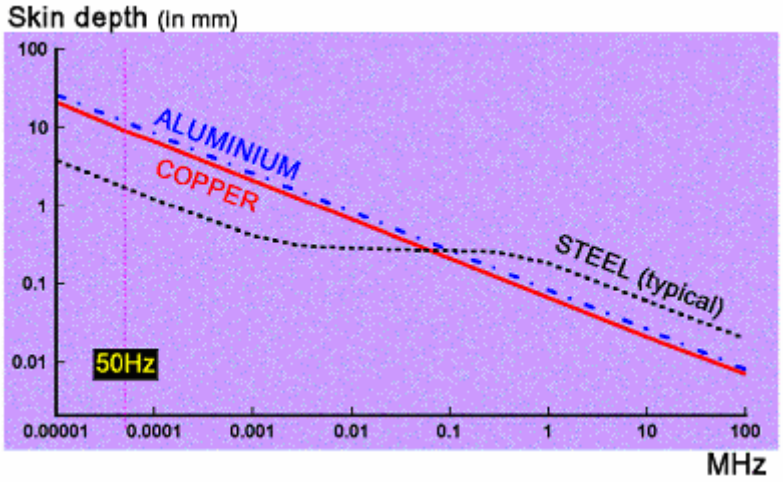

Figure: Graph of Skin Depths for Copper, Aluminium, and Steel

Fuel System: The fuel cell in the aircraft is an 18oz polymer tank that is produced by du-bro. The engine has an integrated fuel pump so the need for a pressure feed is not necessary as for which would be needed with a small nitro methane engine. Flight time has been a major issue during the design phase, so a gasoline powered engine vs. a nitro methane engine was chosen as a power plant because of it fuel efficiency. The estimated flight time of the UAV will be 35 minutes on a full fuel cell.

Engine	**Fuel Consumption**
Zenoah G-26 Gasoline two stroke	1/2 oz./min.
O.S. 1.2 Nitro methane four stroke	1 oz./min.
O.S. .91 Nitro Methane two stroke	1.7 oz./min

Table 1 Engine Fuel Consumption

Mechanical vibration isolation: During the construction and the testing of the prototype UAV we ran into several difficulties. The greatest difficulty that we had to face was vibration. Because the engine that was fitted to the aircraft is a single cylinder engine, it caused a vibration great enough to effect the gyros. The two solutions that were possible at this point were to isolate the vibration source or to update the gyros to a higher quality one such as a ring gyro. Due to the cost of the ring gyro and the equipment needed to integrate it into the MicroPilot board it was decided to attack the vibration problem by isolating the vibration. The first step that we took was placing the MicroPilot case on a bed of vibration absorbent foam. After several field tests it was found that the foam was not protecting the gyros from the vibration. So the next step was to isolate the engine from the airframe. This task was completed by a set of Vibra Lock isolator mounts. This required removal of the engine and modifications of the firewall in order to successfully configure the isolator mounts to the engine and airframe. Once this was completed

we once again performed field tests and the outcome was successful.

The second problem that was faced was the landing gear configuration on the aircraft. The gear consisted of two front wheels and a steer able wheel in the tail of the aircraft. The take off and the landing characteristics of the aircraft were very unstable; as the aircraft would gain or loose speed the tail wheel would come off the ground and the aircraft would be unable to steer as the front two wheel were still on the ground. We felt that to change the configuration of the aircraft to a front steer able wheel would solve these stability issues. With tricycle style gear all three of the wheels will leave the ground close to the same time and the ability to maneuver the aircraft on the ground was greatly improved.

The initial fuel cell that was equipped on the airframe was a 12 fuel cell. Due to the length of the mission, this size tank was not acceptable; it gave the UAV a flight time of 24 minutes. This flight time is well below the necessary time needed to complete the mission.

5. Feedback Control System Design

As mentioned previously it was decided that a prefabricated autopilot system would be used. This would cut down on the time necessary to implement it into an aircraft. The MicroPilot utilizes a Reactive Paradigm to accomplish its task, get to specific locations efficiently. In essence all that the system does is detects deviations or errors in certain flight conditions, compares it to what is desired and reacts. The way in which this is accomplished is by utilizing its Inertial Navigation System in conjunction with the GPS to detect an error. Once an error is "seen", simple PID or PID + feed forward controllers react, control the actuators and put the aircraft back on course. In addition to this, there are other features that are pre-programmed into the MicroPilot, such as when to operate in certain modes. This still however is in the classification of reactive because when certain conditions are met, the MicroPilot will switch modes, it just reacts on a very low level; it is hard to classify anything that the MicroPilot does as a Hierarchical Paradigm for its autonomous operations, everything is Reactive.

5.1 Modeling of PolyUAV

The plane with all the instrumentation is considered as a rigid body and its dynamics is modeled in a body fixed right-hand orthogonal coordinate system with the origin at the center of gravity (c.g.) as shown in Fig. 5.1. The X -axis and the Z -axis are on the symmetry plane of the aircraft with the positive X direction pointing the nose of the aircraft, the positive Y direction pointing to the right wing and the positive Z direction pointing downward.

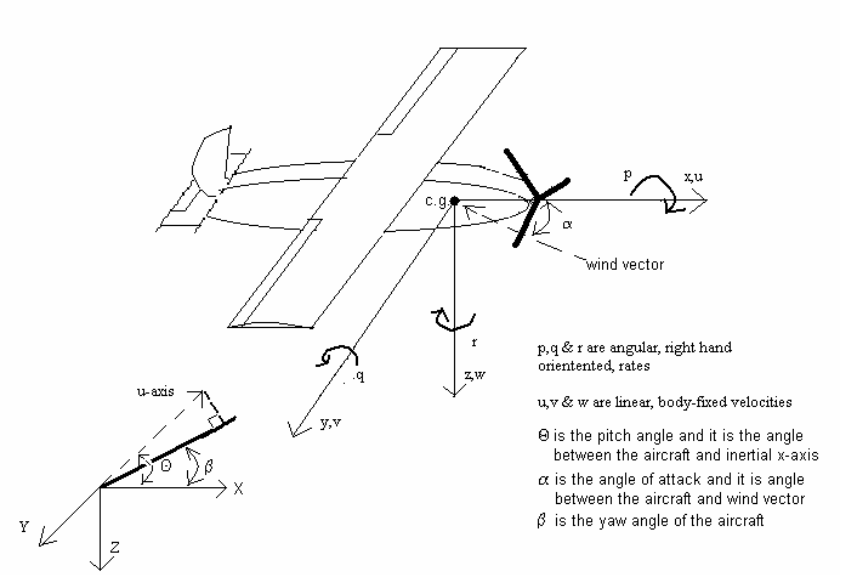

Figure 5.1: Body Fixed Coordinate System Description

In figure 5.1, the coordinate systems are explained. There are a few matters that need to be noted upon and explained. Aerodynamic coefficients are often given in terms of angle of attack. Angle of attack is basically the angle that the front of the aircraft makes with the wind vector (direction the wind, relative to the front of aircraft, is blowing). There are some other angles that are often used as well however. The pitch angle and yaw angle are looked at from an inertial reference frame (earth fixed [shown in lower left corner]). The pitch angle is the angle the aircraft makes with the horizon or the inertial X-axis on the X-Z plane. The yaw angle is the angle that the airplane makes with the X-axis when projected onto the X-Y plane.

Define $\vec{i}$, $\vec{j}$ and $\vec{k}$ be the unit vectors in the X, Y and Z direction, respectively. And, let the velocity of the c.g., $\vec{V}$, and the angular velocity of the aircraft, $\vec{\omega}$, be each expressed in terms of the components in the body coordinate system as

$$\vec{V} = u\vec{i} + v\vec{j} + w\vec{k} \tag{1.1}$$

and

$$\vec{\omega} = p\vec{i} + q\vec{j} + r\vec{k}. \tag{1.2}$$

Then, the dynamics of the aircraft can be obtained by applying the Newton's Second Law for the translational motion and Euler's Equation for the rotational motion. Let $\vec{F}$ be the sum of all the external forces acting on the aircraft including aerodynamics forces and gravitational forces. Then, from the Newton's Second Law, we have

$$\begin{aligned} \vec{F} &= \frac{d}{dt}\left(m\vec{V}\right) \\ &= m\left(\frac{du}{dt}\vec{i} + \frac{dv}{dt}\vec{j} + \frac{dw}{dt}\vec{k} + \vec{\omega}\times\left(u\vec{i} + v\vec{j} + w\vec{k}\right)\right) \\ &= m\left(\frac{du}{dt}\vec{i} + \frac{dv}{dt}\vec{j} + \frac{dw}{dt}\vec{k} + pv\vec{k} - pw\vec{j} - qu\vec{k} + qw\vec{i} + ru\vec{j} - rv\vec{i}\right), \end{aligned} \tag{1.3}$$

where, m is the total mass of the aircraft and all the onboard instruments. Note that in Eq. (1.3),

we ignored the fuel consumption during flight and assumed m to be a constant.

Let F_x, F_y and F_z be the X, Y and Z component of the total force $\vec{F}$, respectively, that is,

$$\vec{F} = F_x\vec{i} + F_y\vec{j} + F_z\vec{k}. \tag{1.4}$$

Then, from Eqs. (1.3) and (1.4), we have

$$\begin{aligned} F_x &= m\left(\dot{u} + qw - rv\right) \\ F_y &= m\left(\dot{v} + ru - pw\right). \\ F_z &= m\left(\dot{w} + pv - qu\right) \end{aligned} \tag{1.5}$$

The rotational motion can be modeled by using Euler's Equation

$$\vec{M}_{total} = \frac{d\vec{H}}{dt}, \tag{1.6}$$

where, $\vec{M}_{total}$ is the total moment about the c.g. and $\vec{H} = I\vec{\omega}$ is the total angular momentum about the c.g. with

$$I = \begin{bmatrix} I_x & -I_{xy} & -I_{xz} \\ -I_{yx} & I_y & -I_{yz} \\ -I_{zx} & -I_{zy} & I_z \end{bmatrix} \tag{1.7}$$

representing the momentum matrix. Then,

$$\begin{aligned} H_x &= pI_x - qI_{xy} - rI_{xz} \\ H_y &= -pI_{xy} + qI_y - rI_{yxz} \\ H_z &= -pI_{xz} - qI_{yz} + rI \end{aligned} \tag{1.8}$$

where

$$\vec{H} = H_x\vec{i} + H_y\vec{j} + H_z\vec{k}. \tag{1.9}$$

Let $\vec{M}_{total}$ be expressed in the component form in the body fixed coordinate systems as

$$\vec{M}_{total} = L\vec{i} + M\vec{j} + N\vec{k}\ . \tag{1.10}$$

By substituting Eqs. (1.8), (1.9) and (1.10) into Eq. (1.6), we have

$$L\vec{i} + M\vec{j} + N\vec{k} = \frac{dH_x}{dt}\vec{i} + \frac{dH_y}{dt}\vec{j} + \frac{dH_k}{dt}\vec{k} + \vec{\omega}\times\left(H_x\vec{i} + H_y\vec{j} + H_z\vec{k}\right) \tag{1.11}$$

From Eqs. (1.2), (1.8) and (1.11), we obtain

$$\begin{aligned} L &= \dot{p}I_x - \dot{q}I_{xy} - \dot{r}I_{xz} - qpI_{xz} - q^2I_{yz} + qrI_z + rpI_{xy} - rqI_y + r^2I_{yz} \\ M &= -\dot{p}I_{xy} + \dot{q}I_y - \dot{r}I_{yz} + prI_x - rqI_{xy} - r^2I_{xz} + p^2I_{xz} + pqI_{yz} - prI \\ N &= -\dot{p}I_{xz} - \dot{q}I_{yz} + \dot{r}I_z - p^2I_{xy} + pqI_y - rpI_{yz} - qpI_x + q^2I_{xy} + qrI_{xz} \end{aligned} \tag{1.12}$$

Then, Eqs. (1.5) and (1.12) completely describe the dynamics of the UAV system given that the total force, $\vec{F} = F_x\vec{i} + F_y\vec{j} + F_z\vec{k}$, and the total momentum about the c.g., $\vec{M}_{total} = L\vec{i} + M\vec{j} + N\vec{k}$, are specified.

Fixed wing aircrafts fly by generating a lift. A simple explanation of how this lift is generated is that it is a consequence of conservation of mass and Bernoulli's equation. In level operation with a cambered (curved on the top) airfoil, the increased velocity over the top of the wing causes the pressure of the top lower than that of the bottom, and this pressure difference between the top and the bottom creates a lifting force. Besides this lifting force, there is a drag force created, opposing the motion of the wing relative to the air. These lift and drag forces are the essence of all the aerodynamic forces: the changes of the wing (including its attachments) geometry alter the airflow over the wing and thus changing the lift and draft forces; and different configurations of the aircraft produce different forces and moments. The way in which an aircraft is able to maneuver in the air is by the use of control surfaces (such as ailerons, elevator, rudder and flaps) to produce moments about the center of gravity thus changing the orientation of the plane. These control surfaces work by the same principal as a wing in general, changing the lift and drag by altering the angle at which it hits the air. The location and motion of these actuators (control surfaces) determine the kind of resulting moments and thus changes of the orientation of the plane. For example, the left and right ailerons acting in opposite directions roll the aircraft; the elevator on the tail section which is symmetric about the X axis produces a pitching moment; and, the rudder which is vertically installed to the tail produces a yawing moment.

For aircraft, the external forces are contributed from two sources, the gravity and the aerodynamic interaction of the aircraft with the environment. The gravitational force is present all the time and it is approximated to be pointing to the center of the earth. On the other hand, the aerodynamic forces are a lot more involved due to the fact that they are complicated nonlinear functions of environmental parameters as well as the states of the aircraft itself. They can be determined analytically, or computationally or experimentally. The analytical methods usually results in very complicated nonlinear models which depends on many aerodynamic coefficients. Those aerodynamic coefficients are determined experimentally under strictly controlled conditions and they usually have large errors if applied to natural environments. Experimental methods are needs specialized equipments such as wind tunnel experimental setup and time consuming. In this project, we decided to use linearized model for the total external force and the total moment as shown below.

$$\begin{aligned} F_x &= F_{x0} + \frac{\partial F_x}{\partial u}\Delta u + \frac{\partial F_x}{\partial v}\Delta v + \frac{\partial F_x}{\partial w}\Delta w + \frac{\partial F_x}{\partial p}\Delta p + \frac{\partial F_x}{\partial q}\Delta q \\ &\quad + \frac{\partial F_x}{\partial r}\Delta r + \frac{\partial F_x}{\partial \delta_{rud}}\Delta\delta_{rud} + \frac{\partial F_x}{\partial \delta_{ail}}\Delta\delta_{ail} + \frac{\partial F_x}{\partial \delta_{elev}}\Delta\delta_{elev} + \frac{\partial F_x}{\partial \delta_{thr}}\Delta\delta_{thr} \end{aligned} \tag{1.13}$$

$$\begin{aligned} F_y &= F_{y0} + \frac{\partial F_y}{\partial u}\Delta u + \frac{\partial F_y}{\partial v}\Delta v + \frac{\partial F_y}{\partial w}\Delta w + \frac{\partial F_y}{\partial p}\Delta p + \frac{\partial F_y}{\partial q}\Delta q \\ &\quad + \frac{\partial F_y}{\partial r}\Delta r + \frac{\partial F_y}{\partial \delta_{rud}}\Delta\delta_{rud} + \frac{\partial F_y}{\partial \delta_{ail}}\Delta\delta_{ail} + \frac{\partial F_y}{\partial \delta_{elev}}\Delta\delta_{elev} + \frac{\partial F_y}{\partial \delta_{thr}}\Delta\delta_{thr} \end{aligned} \tag{1.14}$$

$$\begin{aligned} F_z &= F_{z0} + \frac{\partial F_z}{\partial u}\Delta u + \frac{\partial F_z}{\partial v}\Delta v + \frac{\partial F_z}{\partial w}\Delta w + \frac{\partial F_z}{\partial p}\Delta p + \frac{\partial F_z}{\partial q}\Delta q \\ &\quad + \frac{\partial F_z}{\partial r}\Delta r + \frac{\partial F_z}{\partial \delta_{rud}}\Delta\delta_{rud} + \frac{\partial F_z}{\partial \delta_{ail}}\Delta\delta_{ail} + \frac{\partial F_z}{\partial \delta_{elev}}\Delta\delta_{elev} + \frac{\partial F_z}{\partial \delta_{thr}}\Delta\delta_{thr} \end{aligned} \tag{1.15}$$

$$L = L_0 + \frac{\partial L}{\partial u}\Delta u + \frac{\partial L}{\partial v}\Delta v + \frac{\partial L}{\partial w}\Delta w + \frac{\partial L}{\partial p}\Delta p + \frac{\partial L}{\partial q}\Delta q + \frac{\partial L}{\partial r}\Delta r + \frac{\partial L}{\partial \delta_{rud}}\Delta\delta_{rud} + \frac{\partial L}{\partial \delta_{ail}}\Delta\delta_{ail} + \frac{\partial L}{\partial \delta_{elev}}\Delta\delta_{elev} + \frac{\partial L}{\partial \delta_{thr}}\Delta\delta_{thr} \quad (1.16)$$

$$M = M_0 + \frac{\partial M}{\partial u}\Delta u + \frac{\partial M}{\partial v}\Delta v + \frac{\partial M}{\partial w}\Delta w + \frac{\partial M}{\partial p}\Delta p + \frac{\partial M}{\partial q}\Delta q + \frac{\partial M}{\partial r}\Delta r + \frac{\partial M}{\partial \delta_{rud}}\Delta\delta_{rud} + \frac{\partial M}{\partial \delta_{ail}}\Delta\delta_{ail} + \frac{\partial M}{\partial \delta_{elev}}\Delta\delta_{elev} + \frac{\partial M}{\partial \delta_{thr}}\Delta\delta_{thr} \quad (1.17)$$

$$N = N_0 + \frac{\partial N}{\partial u}\Delta u + \frac{\partial N}{\partial v}\Delta v + \frac{\partial N}{\partial w}\Delta w + \frac{\partial N}{\partial p}\Delta p + \frac{\partial N}{\partial q}\Delta q + \frac{\partial N}{\partial r}\Delta r + \frac{\partial N}{\partial \delta_{rud}}\Delta\delta_{rud} + \frac{\partial N}{\partial \delta_{ail}}\Delta\delta_{ail} + \frac{\partial N}{\partial \delta_{elev}}\Delta\delta_{elev} + \frac{\partial N}{\partial \delta_{thr}}\Delta\delta_{thr} \quad (1.18)$$

Note that in Eqs. (1.13-1.18), the static terms, F_{x0}, F_{y0} and F_{z0}, contain the effect of the gravitational force.

5.2 Identification of system parameters

The system model described by Eq. (1.5) and Eqs. (1.12-1.18) contains system parameters such as inertial parameters and dimensional parameters as well as aerodynamic coefficients. The dimensional parameters were measured, the inertial parameters were calculated by hand and the aerodynamic coefficients were found using computational fluid dynamics (CFD) software. The measured dimensional parameters are given in table 5.1

Demensions	Measurements
Main Wing displacement from front	0.33 m
Main Wing Chord length	.3491 m
Main Wing span	2.34 m
Aileron span	0.61 m
Aileron Chord length	0.07 m
Horizontal Stabilizer displacement from front	1.47 m
Horizontal Stabilizer Span	0.7 m
Elevator span	0.7 m
Horizontal Stabilizer Chord	0.28 m
Elevator Chord	0.11 m
Vertical Stabilizer displacement from front	1.47 m
Vertical Stabilizer Span	0.10 m
Rudder Span	0.10 m
Vertical Stabilizer Chord	0.30 m

Rudder Chord	0.27 m

Table 5.1: Dimensional Parameters of the Aircraft

5.2.1 Obtaining inertial parameters

The total mass of the instrumented aircraft is measured and the location of the center of gravity is based on what is specified by the manufacturer as being necessary for aircraft stability. By adjusting the different component locations inside the aircraft and adding weights to the tail when necessary this was accomplished. The center of gravity turned out to be at a location centered in between the wings on the y–axis and 0.46 m back from the nose of the aircraft on the x-axis. The z-axis location is a little ambiguous and was approximated as being 0.18 m down from the top of the aircraft.

The moment of inertial matrix is calculated by approximate numerical integration. First, the plane is split into 4 components: body, main wings, tail wings and rudder. Each section is then further broken up into simpler geometrical shapes to simplify the calculations. For each section of each component, the elements of the moment of inertial matrix are calculated and the total moment of inertial matrix is obtained by summing those of each sections. The airplane body and the two main wings are mainly hollow with thick walls. The moments of inertia for the body and main wings are calculate by first calculating the moments of inertia obtained by treating them as solid rigid bodies and using the outer dimensions and then by subtracting the moments of inertia obtained by using inner dimensions. The tail wings and rudder are made from thin materials and the moments of inertia are therefore obtained by treating them as two dimensional objects. Care is taken to take into account empty spaces between the ribs of the wings and holes in the wood by appropriately adjusting equivalent density of the material. The calculated values for the elements of the moment of inertia matrix are given in table 5.2.

Inertial Parameters	**Calculated Values**
Mass of aircraft*	7.62 kg
Ix	0.5528 $kg.m^2$
Iy	0.6335 $kg.m^2$
Iz	1.0783 $kg.m^2$
Ixy = Iyx	0
Ixz = Izx	$1.507x10^{-3}$ $kg.m^2$
Iyz = Izy	0

Table 5.2: Inertial Parameters; (*) is measured.

5.2.2 Obtaining Aerodynamic Coefficients

The aerodynamic coefficients; the constant terms and the partial derivatives in Eqs. (1.12-1.18), need to be determined for the specific aircraft used here. We obtained all the aerodynamic coefficients by using a program, TORNADO (Reference [7]). It is a MATLAB based computational fluid dynamics program that uses the Vortex Method to calculate aerodynamic coefficients for different flight conditions.

In order to utilize this software much had to be done because the TORNADO program requires that each wing be constructed from data such as the reference location and base chord length.

These dimensional values had to be measured and were. The next step was to split the different lifting surfaces into partitions; the more partitions the greater the accuracy of the coefficients that will be outputted, however the calculations will be more time consuming. For our purposes, the main wing was split into 4 partitions. The first represents the main body of the wing, while the other three describe the geometry of the wing tip. The control surfaces also had to be input into the wing description so that the corresponding aerodynamic coefficients could be calculated by the software. For the main wing only 1 of the partitions was specified as a control surface and it represents the ailerons. Even though modeling the shape of the wings was very important, the most important part would have to be the NACA airfoil number assigned to each specific wing partition. This is how the TORNADO program is able to calculate the forces. After careful measurement, the main wing was determined to have an airfoil with a NACA number of 2314. It was also realized that the camber tended to decrease near the tip, so this had to be accounted for as well and was by gradually decreasing the thickness corresponding to the last two numbers of the NACA number.

The other two wing surfaces that were defined were the horizontal and vertical stabilizers. The horizontal stabilizer was split into 4 partitions. In addition to this, the elevator is a part of the horizontal stabilizer and had to be implemented into it. The vertical stabilizer was split into 3 partitions and it is comprised of the rudder as well. To define the elevator, all 4 of the horizontal stabilizer partitions were "flapped" (TORNADO terminology), thus making up the elevator (when obtaining coefficients from these, the results were added together to represent the entire control surface). To define the rudder, all 3 of the partitions on the vertical stabilizer were "flapped". For both of these wing surfaces, the NACA number was defined to be 0002, the reason for this is that these wing sections are symmetric and quite thin. At zero angle of attack they produce no lift; they only produce lift when there is an angle with the wind vector other than zero. A representation of the aircraft after it was modeled is displayed in Figure 5.1.

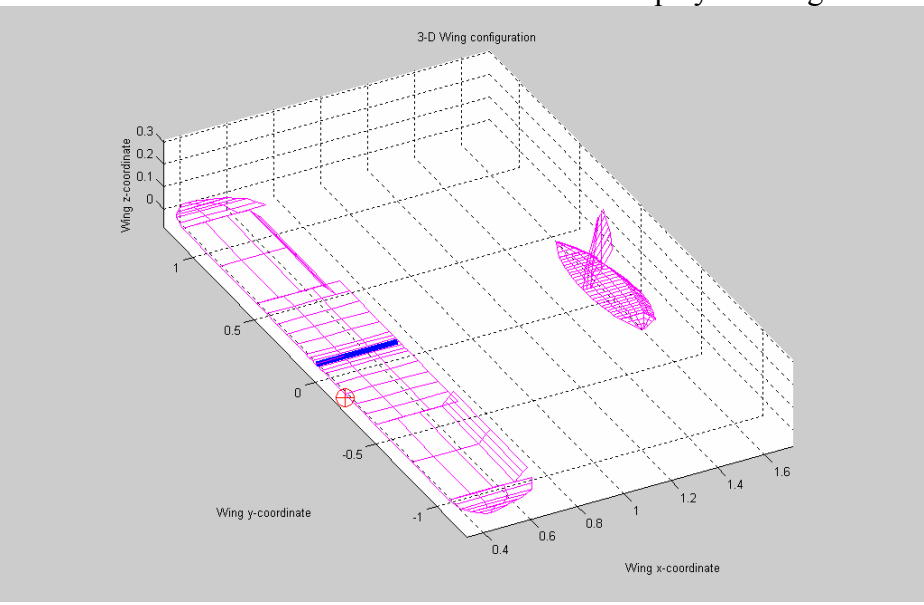

Figure 5.1: Model of Lifting Surfaces for Aircraft

Once the geometry was specified in the TORNADO program, it was necessary to actually run the simulation thus obtaining the necessary aerodynamic coefficients. This program gives a

linear representation of the coefficients (it only gives a first order derivative) thus a specific operating point must be specified and the slope at that condition will be obtained. Because of this, a few different runs of the TORNADO program were depending on different the flight conditions (such as climb and descent). The coefficients obtained can all be viewed in Table 5.2a. By normal aerodynamic convention, the numbers given have been non-dimensionalized. In order to put it in the form that we need for our equations, they have to be multiplied by the corresponding non-dimensionalization factor. The different non-dimensionalization factors can be found in Table 5.2b.

Parameters	**Level Flight**	**Climb**	**Descent/Landing**
Average airspeed over all of flight condition	10.28 m/s	11.1 m/s	15.7 m/s
Average angle over all of flight condition	-1 degrees	15 degrees	-5 degrees
$CF_{x\,0}$	-.0024	-.0024	-.0024
$CF_{x\,\alpha}$	-.04426	-.60	.098346
$CF_{x\,q}$	.00818	1.99	-.5144
$CF_{x\,elev.}$	.0138	.159	.054019
$CF_{y\,\beta}$	-.31591	-.3587	-.30364
$CF_{y\,p}$	.051422	.0607	.032853
$CF_{y\,r}$	.43656	-.308458	.41958
$CF_{y\,ail.}$	.041708	.0167	.037081
$CF_{y\,rud.}$	-.236731	-.308458	-.219213
$CF_{z\,0}$	-.3676	-.3676	-.3676
$CF_{z\,\alpha}$	-5.4596	-5.2428	-5.4645
$CF_{z\,q}$	-22.7608	-24.5912	-22.917
$CF_{z\,elev.}$	-.54998	-.57583	-.55575
CL_{β}	-.033675	-.033508	-.032649
CL_{p}	-.64379	-.67943	-.64654
CL_{r}	.091493	.32236	-.034349
$CL_{ail.}$	-.388	-.389	-.387
$CL_{rud.}$	.0249895	.02978	.02354
CN_{β}	-.14132	-.16411	-.13511
CN_{p}	-.0191396	-.25076	.061242
CN_{r}	-.19704	-.22984	-.18909
$CN_{ail.}$	-.0062179	-.025607	.0078
$CN_{rud.}$	-.109659	-.145211	-.101163
CM_{0}	-.0508	-.0508	-.0508
CM_{α}	-.66058	-.66058	-.35577
CM_{q}	-14.7974	-20.5082	-13.8432
$CM_{elev.}$	-.167194	-1.80456	-1.69754

Table 5.2a: Aerodynamic Coefficients

Q	$= 1/2\rho u^2$ (ρ) is density
Derivatives of Forces w.r.t. anything except p, q, r	Non – dimensionalization factor: (Q)(Wing Area)
Derivatives of Moments w.r.t. anything except p, q, r	Non – dimensionalization factor: (Q)(Wing Area)(Wing Span)
Derivatives of Forces w.r.t. p	Non – dimensionalization factor: (Q)(Wing Area)(1/u)(1/2)(Wing Span)
Derivatives of Forces w.r.t. q	Non – dimensionalization factor: (Q)(Wing Area)(1/u)(Chord Length)
Derivatives of Forces w.r.t. r	Non – dimensionalization factor: (Q)(Wing Area)(1/u)(1/2)(Wing Span)
Derivatives of Moments w.r.t. p	Non – dimensionalization factor: (Q)(Wing Area)(1/u)(1/2)(Wing Span)^2
Derivatives of Moments w.r.t. q	Non – dimensionalization factor: (Q)(Wing Area)(Wing Span) (1/u)(1/2)(Chord Length)
Derivatives of Moments w.r.t. r	Non – dimensionalization factor: (Q)(Wing Area)(1/u)(1/2)(Wing Span)^2

Table 5.2b: Non-dimensionalization parameters

5.3 Controller design

Linear control model: Now that the equations of motion had been formed, with these six equations it was now possible to start putting the system together in MATLAB. As for the force and moment terms that are dependent upon the current state of the aircraft, the Taylor Expansion representation calculated earlier was used and all the aerodynamic coefficients and moments of inertia were implemented.

All of these equations were then easily implemented in MATLAB. The ease of implementation is a direct result of the fact that MATLAB has the capability of converting a non-linear system in Simulink to a linear State Space form. It was thus necessary to define the entire system in block diagram form in MATLAB. All the equations of motion were put together, and all forces attributed. Once the block diagram is formed, the state space model is obtained from the non-linear block diagram and it can then be converted into individual transfer functions corresponding to the open loop transfer functions of the system. All of this was done using simple MATLAB functions. First, the TRIM command had to be used to determine the state variables corresponding to the initial conditions that had to be specified so that MATLAB would be able to linearize the system (as with any linearization, a specific operating point is needed). This operating point that was specified by us depended on the transfer functions that were required. The TRIM command outputted the vectors that would be used in conjunction with the LINMODV5 command (this is the linearization algorithm that was chosen). This command is what actually linearizes the block diagram and puts it into a state space form around the specified operating point. The reason LINMODV5 was chosen is that it is a newer version than LINMOD and LINMOD2, it has a couple of the bugs worked out and is a little more accurate. Once the state space system was created, this could be converted into open loop transfer functions using the SS2TF command. The lateral equations were then compared to the method done nearly

entirely by hand and corrected until they both made sense and checked. Of course they would not be exact because the second method is more accurate, however the general trends should be similar and they were.

PID controller design: The next step in this process was to determine the control coefficients that would be used in the PID controllers for MicroPilot. Although, we have defined the entire aircraft including all control surfaces and their interactions with all other variables, MicroPilot is not this advanced and only allows certain Transfer functions to be used and they are mostly in the form of a single input and single output.

MicroPilot accommodates 11 transfer function control feedback loops. All of these have the capability of proportional, derivative and integral control. In addition to this, a few feedback loops have a feed forward control coefficient as well. The feed forward coefficient is mainly used for transfer functions that have a necessary coupling between the aileron and rudder. This feed forward component complicates things quite a bit and with the time restraint it would be very difficult to calculate analytically. Because of this it was decided to calculate only the PID gains analytically and any feed forward components experimentally. The 11 transfer functions that MicroPilot utilizes are as follows: aileron from roll, elevator from pitch, rudder from Y – acc., rudder from heading, throttle from speed, throttle from altitude, pitch from altitude, pitch from AGL, pitch from airspeed, roll from heading and heading from cross track error.

One must keep in mind that not all of these are used at one specific set of flying conditions. For example, pitch can be controlled by both the airspeed and the elevator. Depending on whether the airplane is in a landing scenario or a level flight scenario the transfer function used would be different. In addition to this, some of the transfer functions are cannot be directly obtained from the rudimentary model that we have and need to be done experimentally. An example of this is anything involving thrust. Thrust is not a result of the aircraft geometry and the manufacturer does not give all the necessary information to model it. For this reason it would be necessary to obtain the specific "aerodynamic" coefficients relating to this experimentally, then put that in the model and obtain the transfer functions. With the time constraint it would be most practical to do this from a more experimental standpoint.

All of the transfer functions were calculated first by determining, analyzing and agreeing at its correctness the open loop transfer functions. From this a control feedback loop was created and the best control coefficients determined. The first loop studied was the elevator from pitch transfer function for level flight and here it is:

$$\frac{\Delta\theta}{\Delta\delta_{elev.}} = \frac{100s^6 + 3300s^5 + 20510s^4 - 37830s^3 - 344220s^2 + 12420s + 10060}{s^8 + 54s^7 + 911s^6 + 4527s^5 - 9752s^4 - 87006s^3 + 7332s^2 - 19690s + 4032}$$

The graph of the output can be obtained in Figure 5.3.

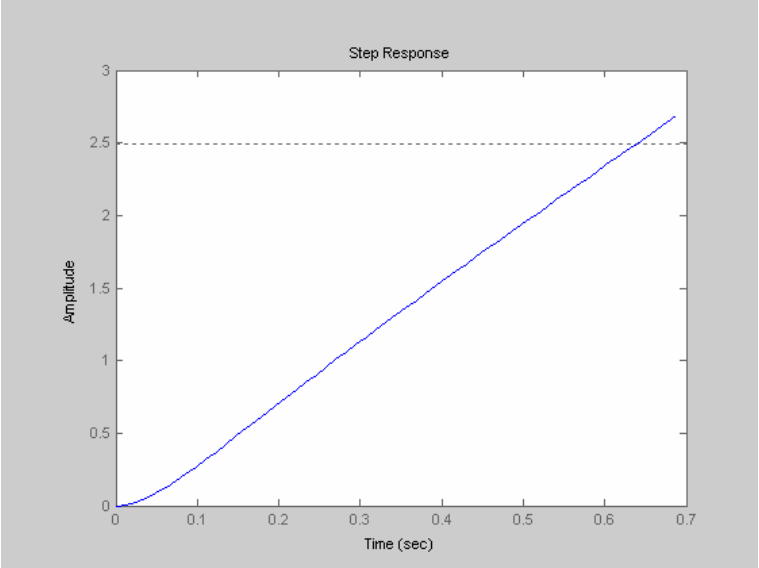

Figure 5.3: Level Flight open loop transfer function for elevator deflection from pitch

Figure 5.3 makes perfect sense in that it is unstable. A deflection of the elevator will cause the pitch angle to increase without bound. As for determining if it makes sense in practice, it is often a very hard task to accomplish. What is looked for s anything outrageous that does not make any sense, such as taking five minutes to change 10 degrees. This graph does not ring any of those bells and therefore is taken to be a good representation.

To properly design a PID feedback system for this obviously unacceptable open loop transfer function (it is unstable and does not suite the function of the controller), the new closed loop transfer function first had to be defined. A representation of the PID control feedback loop to be used is displayed in Figure 5.4.

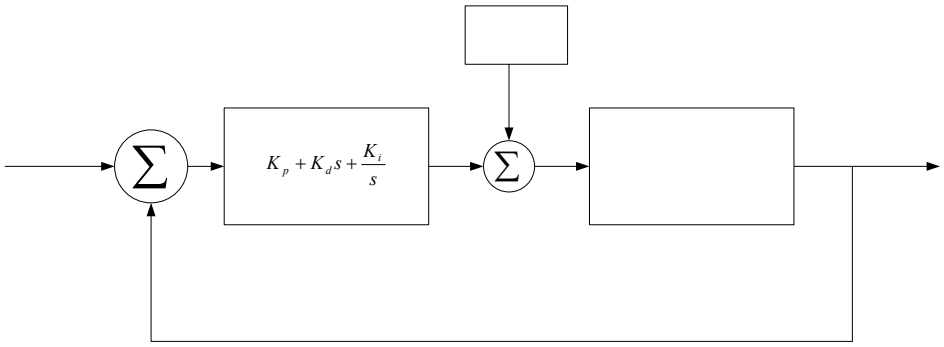

Figure 5.4: Representation of PID control feedback loop

Using this knowledge and with the help of MATLAB, the control gains that make this feedback loop operate most efficiently for our specific plant (in this case, level flight elevator from pitch transfer function). The function used in MATLAB is the cloop function and it creates a closed loop transfer function from a given controller and plant input. A sample piece of code is:

[numcl,dencl]=cloop(conv(num,[-5 -20000 -2000]),conv(den,[1 0]));.

Written mathematically, the form of the closed loop transfer function is:

$$G_{CL}(s) = \frac{(PLANT)\left(K_P + K_D s + \frac{K_I}{s}\right)}{1 + (PLANT)\left(K_P + K_D s + \frac{K_I}{s}\right)}$$

And the Characteristic Equation is:

$$1 + (PLANT)\left(K_P + K_D s + \frac{K_I}{s}\right) = 0$$

For this specific case, when defining coefficients of Kp= 10 000 Kd= 80 Ki = 1 000, the step response of the closed loop system created first by defining the non-linear Simulink block diagram becomes what is displayed in Figure 5.5:

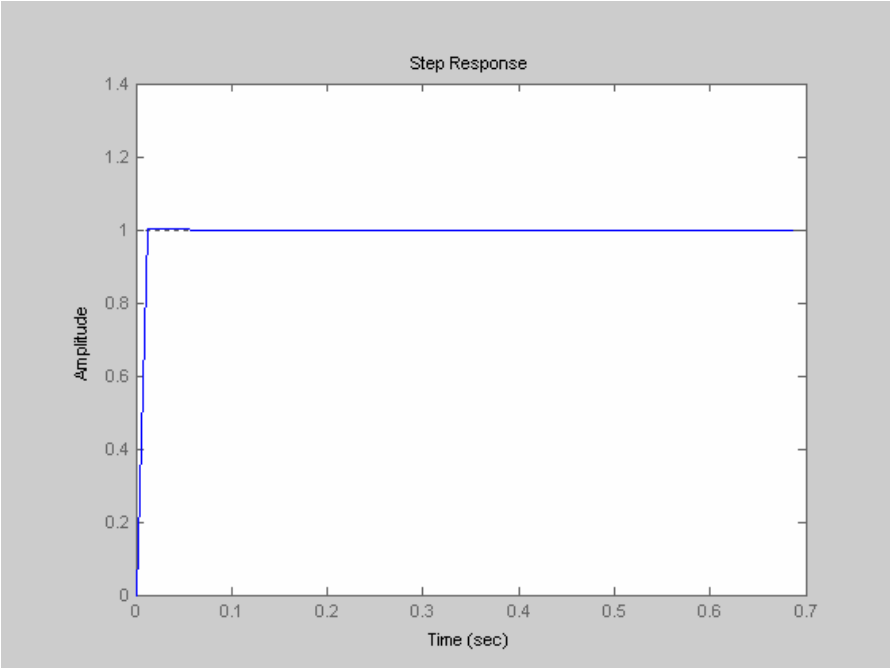

Figure 5.5: Closed loop Transfer Function for elevator from pitch transfer function for level flight

As can be seen from Figure 5.5, the system has become stable. Not only is it stable, but it has very little overshoot and a very quick settling time. In theory, with these gains, the elevator from pitch control system should work very well for level flight.
The other PID gains that were analytically calculated were done in a very similar fashion and are shown below.

<u>Transfer functions and PID gains:</u>

Level Flight:

$$\frac{\Delta\theta}{\Delta\delta_{elev.}} = \frac{100s^6 + 3300s^5 + 20510s^4 - 37830s^3 - 344220s^2 + 12420s + 10060}{s^8 + 54s^7 + 911s^6 + 4527s^5 - 9752s^4 - 87006s^3 + 7332s^2 - 19690s + 4032}$$

Kp= 10,000 Kd= 80 Ki= 1,000

$$\frac{\Delta Y - acc.}{\Delta\delta_{rud.}} = \frac{200s^7 + 14840s^6 + 239830s^5 + 981630s^4 + 59810s^3 + 260220s^2 - 21790s}{s^8 + 54s^7 + 911s^6 + 4527s^5 - 9752s^4 - 87006s^3 + 7332s^2 - 19690s + 4032}$$

Kp= 20,000 Kd= 0 Ki= 4,000

$$\frac{\Delta roll}{\Delta \delta_{ail.}} = \frac{170s^6 + 5130s^5 + 33770s^4 - 46780s^3 - 633190s^2 - 73960s - 179750}{s^8 + 54s^7 + 911s^6 + 4527s^5 - 9752s^4 - 87006s^3 + 7332s^2 - 19690s + 4032}$$

Kp= 20,000 Kd= 50 Ki= 5,000

$$\frac{\Delta alt.}{\Delta \theta} = \frac{800s^6 + 12600s^5 + 60300s^4 - 142800s^3 - 1169400s^2 + 22430s - 2000}{s^8 + 52s^7 + 865s^6 + 4168s^5 - 9251s^4 - 79452s^3 + 3067s^2 + 2039s}$$

Kp= 8,000 Kd= 80 Ki= 1,000

Climb:

$$\frac{\Delta \theta}{\Delta \delta_{elev.}} = \frac{59s^8 + 1492s^7 + 8998s^6 + 1727s^5 + 34307s^4 + 26855s^3 + 21249s^2}{s^{10} + 47s^9 + 704s^8 + 3564s^7 + 1074s^6 - 14419s^5 + 14822s^4 - 187s^3 + 7747s^2}$$

Kp= 4000 Kd= 25 Ki= 500

$$\frac{\Delta AirSpeed}{\Delta \theta} = \frac{10s^6 + 466s^5 + 6800s^4 + 33090s^3 - 1220s^2 - 157290s + 196420}{s^7 + 47s^6 + 7645s^5 + 3564s^4 + 1041s^3 - 15116s^2 + 12434s + 8320}$$

Kp= 14,000 Kd= 25 Ki= 300

$$\frac{\Delta Y - acc.}{\Delta \delta_{rud.}} = \frac{100s^7 + 7320s^6 + 98420s^5 + 262740s^4 - 58220s^3 + 40260s^2 - 65470s}{s^8 + 47s^7 + 704s^6 + 3564s^5 + 1074s^4 - 14419s^3 + 14822s^2 - 187s + 7747}$$

Kp= 10,000 Kd= 0 Ki= 1,000

$$\frac{\Delta roll}{\Delta \delta_{ail.}} = \frac{-100s^6 - 2790s^5 - 14690s^4 + 17630s^3 + 161580s^2 + 57710s + 63030}{s^8 + 47s^7 + 704s^6 + 3564s^5 + 1074s^4 - 14419s^3 + 14822s^2 - 187s + 7747}$$

Kp= 25,000 Kd= 4000 Ki= 3,000

Descent/Landing:

$$\frac{\Delta \theta}{\Delta \delta_{elev.}} = \frac{120s^6 + 4010s^5 + 26560s^4 - 53120s^3 - 531660s^2 - 63670s + 3690}{60s^7 + 960s^6 + 4720s^5 - 13130s^4 - 107340s^3 - 10090s^2 - 15210s + 680}$$

Kp= 17,000 Kd= 100 Ki= 1,000

$$\frac{\Delta roll}{\Delta \delta_{ail.}} = \frac{200s^6 + 6210s^5 + 41240s^4 - 73040s^3 - 877220s^2 - 115280s - 129360}{60s^7 + 960s^6 + 4720s^5 - 13130s^4 - 107340s^3 - 10090s^2 - 15210s + 680}$$

Kp= 25,000 Kd= 80 Ki=10,000

$$\frac{\Delta Y - acc.}{\Delta \delta_{rud.}} = \frac{200s^6 + 18300s^5 + 309200s^4 + 1316100s^3 + 259900s^2 + 196500s + 9300}{60s^7 + 460s^6 + 4720s^5 - 13130s^4 - 107340s^3 - 10090s^2 - 15210s + 680}$$

Kp= 10,000 Kd= 0 Ki= 1,000

$$\frac{\Delta descent}{\Delta \theta} = \frac{900s^6 + 15300s^5 + 74600s^4 - 217700s^3 - 1726600s^2 + 34200s + 1700}{60s^6 + 960s^5 + 4720s^4 - 13150s^3 - 107880s^2 - 11380s + 680}$$

Kp= 10,000 Kd= 0 Ki= 1,000

$$\frac{\Delta alt.}{\Delta \theta} = \frac{900s^6 + 15300s^5 + 74600s^4 - 217700s^3 - 1726600s^2 + 34200s + 1700}{60s^7 + 960s^6 + 4720s^5 - 13150s^4 - 107880s^3 - 11380s^2 + 680s}$$

Kp= 17,000 Kd= 100 Ki= 800

6. Conclusions and Future Works

The future is bright for the UAV. As computers become smaller and faster and the public becomes more comfortable with computers making critical decisions UAVs will begin to move into the commercial markets and possibly replace commercial airliners as we know them. Organizations such as AUVSI and the competitions that it hosts are helping prepare young engineers for develop the next technological break through in Autonomous Vehicles. At Polytechnic University, MicroPiolot was the autonomous control system used and two twin AIPTEK mini cams is the imaging system. By utilizing these as well as many other small components, Polytechnic University's UAV Project will be a reality soon enough. It is moving along confidently and has not stayed from schedule. The development of the Control Gains, designation of the Imaging System, and completion of the EM Shield are hallmarks of the program, and show that a success at the competition in June is clearly achievable.

References

[1] Robert C. Nelson, "Flight Stability and Automatic Control," McGraw Hill, 1989.

[2] G. F. Franklin, J. D. Powell and A. Emami-Naeini, "Feedback Control of Dynamic Systems," 4th Ed., Prentice-Hall, 2002.
[3] Bernard Etkin and Lloyd Duff Reid, "Dynamics of Atmospheric Flight," 3rd Ed., John Wiley & Sons, 1995.
[4] MicroPilot, "MicroPilot-MP2028g Installation and Operation." 2001.
[5] Spectral Analyzer Tutorial. http://www.bright.net/~kanga/kanga/w7zoi/SA_support_info/SA%20Tutorial.htm
[6] Design Techniques for EMC shielding. Keith Armstrong, Eur Lng http://www.compliance-club.com/archive1/990810.htm
[7] Thomas Melin, "A Vortex Lattice MATLAB Implementation for Linear Aerodynamic Wing Applications," Royal Institute of Technology, Department of Aeronautics, December 2000.

Acknowledgement
We would like to give acknowledgement to several people that have helped us during the design and experimental stages of Polytechnic University's UAV. Professor William McShane who helped get the project moving; he has been a key supporter in the project and will see it to the end. Professor Meihua Tai who gave unlimited support in the areas of control and navigation. The help from Professor Iraj Kalkhoran in the area of aerodynamics and flight stability. Herbert Ruetter from Northrop Grumman Integrated Systems for the support in the areas of unmanned vehicle performance. Thomas Hunt from Northrop Grumman Integrated Systems for his support in the field of aerodynamics. The help that was received from David Wigley from Long Island Skyhawks for the assistance in technical support.